RECENT QCD RESULTS FROM THE TEVATRON*

H. Piekarz

Florida State University, Tallahassee, Florida 32306, U.S.A.

Recent QCD results from the CDF and DØ detectors at the Tevatron $\bar{p}p$ collider are presented. An outlook for future QCD tests at the Tevatron collider is also briefly discussed.

PACS numbers: 12.38. Qk

1. Introduction

Quantum Chromodynamics (QCD) is the SU(3) gauge theory of colored quarks and self-interacting colored gluons. It describes the strong interaction within the *Standard Model* of elementary particles. At hadron colliders, QCD processes occur with large cross-sections strongly dominating all other possible backgrounds. Colored partons from these processes evolve via soft quark and gluon radiation followed by hadronization to form observable colorless hadrons. The Tevatron $\bar{p}p$ collider with its 1.8 TeV center of mass energy allows for investigation of parton interactions in the energy range far beyond the original energies that lead to creation and evolution of QCD. In addition, the increase of the instantanous luminosity up to $2 \times 10^{31} \text{cm}^{-2}\text{sec}^{-1}$ allowed the experiments to accumulate in recent collider run about 100 pb^{-1} of integrated luminosity. Therefore, new QCD results from the Tevatron provide the strongest test yet of the high Q^2 aspect of the model and may open window on physics beyond QCD if deviations from the model are found.

2. Colliding beam detectors and data processing

The colorless hadrons from the final state interaction appear in the detector as localized energy deposits called jets. The hadrons in a jet have small transverse momenta relative to their parent parton's direction and the sum of their longitudinal momenta approximately gives the parent parton

---

momentum. The definition of a jet involves some arbitrariness and may vary from one experiment to another. Good understanding of jet reconstruction efficiency and energy corrections is crucial in preparation of data to compare with theory.

The CDF and DØ detectors are described in [1] and [2], respectively. In both detectors the calorimeter is a central structure with tracking detectors filling the space between the beam line and the electromagnetic section of the calorimeter. The muon detectors cover the outermost area of the hadronic section of the calorimeter. The rapidity coverage is for $|\eta| \leq 4.2$ in DØ detector and for $|\eta| \leq 3.0$ in CDF detector (the pseudo-rapidity is defined as $\eta = -\ln(\tan(\theta/2))$, where θ is the polar angle relative to the colliding beam). The depth of the DØ calorimeter varies from about 6λ at low η to about 13λ for the highest η while the depth of the CDF calorimeter ranges from 4.5λ in the central region to about 7λ in the forward one. The calorimeters are well segmented in both rapidity and azimuthal angle ($\Delta\eta \times \Delta\phi = 0.1 \times 0.1$) facilitating triggering and detection of both single particles and objects like jets. In both CDF and DØ the single particle energy resolution of the electromagnetic section is of the order of $15\%/\sqrt{E}$ while for hadronic section the resolutions are in the range of $80\%/\sqrt{E}$ for CDF and $50\%/\sqrt{E}$ for DØ detector, respectively. In both detectors the hadronic resolution has a significant constant term.

The event selection is made in two subseqent hardware triggers followed by a final software stage. The hardware triggers typically require detection of the transverse energy above a preset threshold in the calorimeter trigger towers. After events are selected the signals are digitized and jets are reconstructed using a fast cone algorithm. As the jet production cross-section spans many orders of magnitude several software jet energy thresholds are applied to avoid saturation of the data acquisition bandwidth with lower E_T events. A careful study of jet detection and reconstruction efficiency, as a function of the jet energy threshold at the trigger level, is required prior to adding the data over a full energy range.

Both detectors also include scintillation hodoscopes located on each side of the interaction region at high η. The timing distribution of particles traversing the two hodoscopes indicates the occurrence of an inelastic interaction during a beam-beam crossing and is used to trigger the remaining sections of the detector. The event vertex is determined using tracks reconstructed in the central tracking system. The high precision silicon tracker at CDF was used in the determination of the primary vertex. At DØ , with a less precise wire chamber tracker, the event reconstruction retained up to two vertices. The quantity, H_T, a scaler sum of all jet's E_T in the event was calculated for both vertices. The vertex with the minimum H_T was used to calculate E_T and η of all jets in the event.

Jets are reconstructed offline using an iterative jet cone algorithm with cone radius of $R=0.7$ in $\eta - \phi$ space. The algorithm uses preclusters formed with seed towers (*e.g.* 1 GeV for DØ). The jet E_T is defined as the sum of each cell E_T within the cone. The E_T -weighted rapidity and azimuth of the jet are calculated giving new center of the cone. The jet E_T and direction are recalculated until the cone direction is stable. The final jet directions are calculated using the components of the jet energy vector. After all jets are formed, closely spaced jets which share more than 50% of the smaller jet energy are merged; otherwise the energy is split evenly between the two.

Cosmic rays, accelerator losses and multiple interactions may constitute severe background and distort both jet selection and reconstruction. At CDF the $\not{E}_T$ significance ($\not{E}_T/\sqrt{E_T} \leq 6.0$) was used to remove cosmic ray and accelerator loss events. The multiple interaction events were removed by requiring that the total E in the event be less than 1.8 TeV. At DØ the cosmic rays and accelerator losses were eliminated by requiring the missing transverse energy in the event, $\not{E}_T$, to be less than 70% of the leading jet E_T. With this cut, residual contamination from the backgrounds was estimated to be less than 2% for all jets with $E_T \leq 500$ GeV.

The measured jet E_T spectrum has to be corrected for the jet energy scale calibration and resolution smearings, including effects of the underlying events and particle energy showering outside the jet cone. The calorimeter hadronic response and resolution smearings are strongly detector dependent and account for most of the systematic errors. The uncertainty in the integrated luminosity also plays a role in determining the systematic error. Physics conclusions are based on comparison of corrected collider data with simulations which are in turn dependent on choice of the program, proton structure functions and other theoretical parameters. We shall discuss some of these effects in more detail when presenting particular physics results.

3. Direct photons

Direct photon production at the Tevatron collider permits a precision test of QCD with relatively small statistical and systematic errors. At lowest order, the dominant production mechanism is quark Compton scattering off a gluon in the initial state. This implies that direct photons provide a way to study the gluon distribution of the photon. In addition, the measurement of diphoton production also tests QCD, and the two-photon final state allows for precise reconstruction of the initial state quantities such as transverse momentum of the system.

In both CDF and DØ experiments photons are identified in the electromagnetic section of the calorimeter. Candidate events are restricted to the calorimeter rapidity range covered with fully instrumented tracking detec-

tors. This permits the elimination of events with a charged track pointing to a candidate cluster. The electromagnetic energy fraction of the calorimeter shower was required to be greater than 89% (CDF) and 96% (DØ). The shower profile had to be consistent with that of test beam electrons helping to suppress π^0 and η backgrounds. In addition the photons were required to be isolated, with less than 2 GeV of transverse energy in an annular region between R=0.2 and R=0.4 (R $= \sqrt{\Delta\eta^2 + \Delta\phi^2}$) around the photon. Finally, the $\not{E}_T$ of the event was required to be less than 20 GeV to reject $W \to e\nu$ decays with electron faking a photon and events with large calorimeter noise. CDF uses a conversion method to distinguish π^0 and η from a single photon event while DØ employs the fraction of EM showers starting in the first two radiation lengths of the calorimeter. At CDF, photons which convert in the magnet coil are detected in the preshower detector. The probability of a photon pair from π^0 or η converting in the magnet coil is higher than for a single photon.
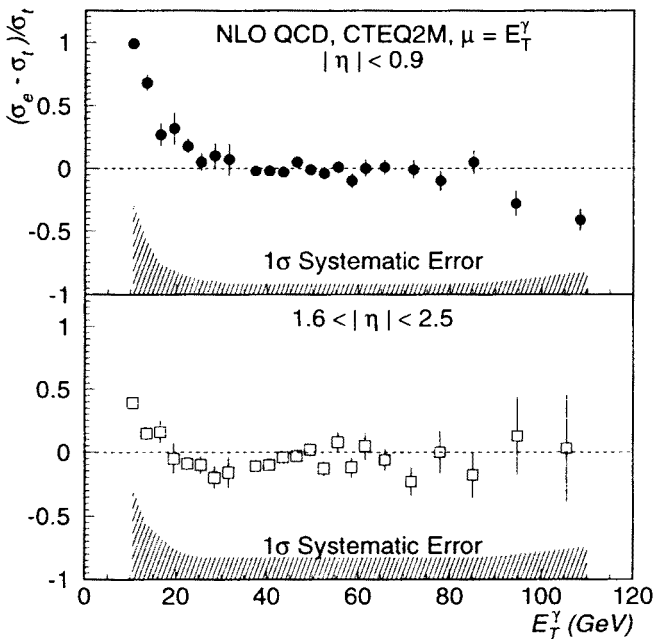

Fig. 1. A comparison of DØ direct photon data with NLO QCD theory, using CTEQ2M parton distributions.

A comparison of DØ inclusive photon data [3] with NLO QCD theory [4] is shown in Fig. 1. The data are divided into two rapidity ranges: central and forward. Some disagreement with theory is observed at low E_T end

and smaller rapidities. The photon purity for DØ is shown in Fig. 2 for low and high rapidity ranges. One should note that purity of the photon sample rapidly decreases as the photon E_T decreases. This leads in turn to a considerable increase of the systematic error at low E_T range as indicated in Fig. 1. The photon purity is not strongly dependent on the rapidity range. The inclusive photon cross-section from CDF [5] covers the energy range from 10 GeV to 120 GeV, and the profile and conversion methods produced similar results. The data are well reproduced by the NLO QCD theory [6] using the CTEQ2M parton distribution functions with a renormalization scale $\mu = P_T$. Detailed examination of the data indicates, however, a possibility of a deviation from the theory for events with photon P_T below about 30 GeV. This deviation seems to be stronger than the one observed at DØ . One proposed explanation is that additional soft radiation [7] beyond the NLO QCD contributes to production of low P_T direct photons. However, due to difficulty of photon identification at low E_T, more statistics is needed to permit the use of stronger suppression of the non-photon backgrounds. This may allow in turn to make more firm conclusion about possibility of deviation from the theory.
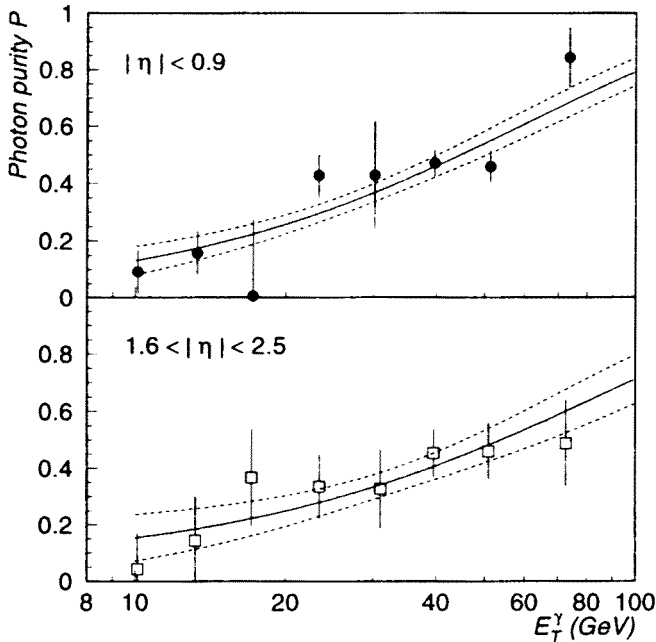

Fig. 2. The DØ photon purity as a function of transverse energy. The errors shown are combined statistical and systematic; the lines indicate the fit and its variation.

Both CDF and DØ also measured the diphoton mass spectrum. At DØ, the candidate events were required to have two photon candidates found within the central region ($|\eta| \leq 1.0$) with leading photon $E_T^1 \geq 14$ GeV and $E_T^2 \geq 13$ GeV. In addition, an invariant mass cut was imposed to remove $Z \rightarrow ee$ events. A differential diphoton mass spectrum from DØ [8] obtained for 80 pb^{-1} is shown in Fig. 3. Data which cover diphoton mass of (40-120) GeV show good agreement with theory at a renormalization scale $\mu = E_T$ using CTEQ2M parton distributions. The CDF result [10] obtained for 84 pb^{-1} (and in the $|\eta| \leq 0.9$) is shown in Fig. 4. The CDF data cover diphoton mass range (30-80) GeV and show good agreement with NLO QCD [9] at $\mu = E_T$ renormalization scale with CTEQ2M parton distributions. In the diphoton mass range where the two experiments overlap, they agree.
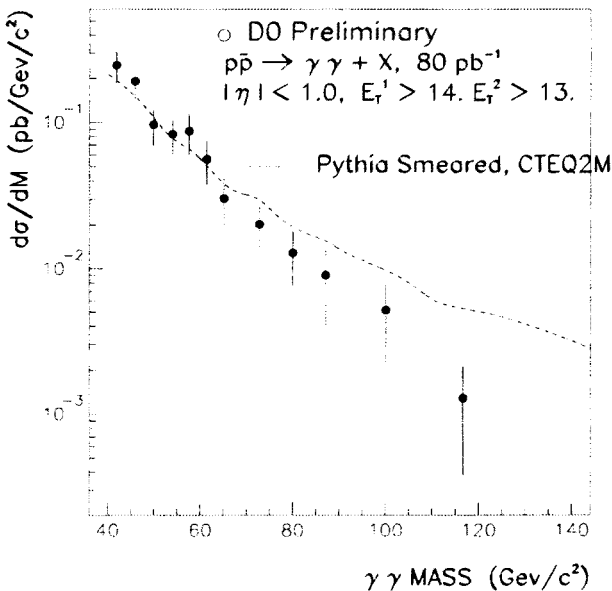

Fig. 3. The diphoton differential cross-section from DØ as a function of the diphoton invariant mass.

In conclusion, we observe that the inclusive photon cross-section in the range of E_T's above 30 GeV shows good agreement with the NLO QCD. At low E_T there is a deviation from the theoretical prediction. This photon energy range, however, suffers from large systematic errors due to difficulty in identification of the photon. Data with higher statistics are needed to allow for imposition of more stringent photon selection rules in order to better purify the photon candidate sample and thus reduce in this way the systematic error.
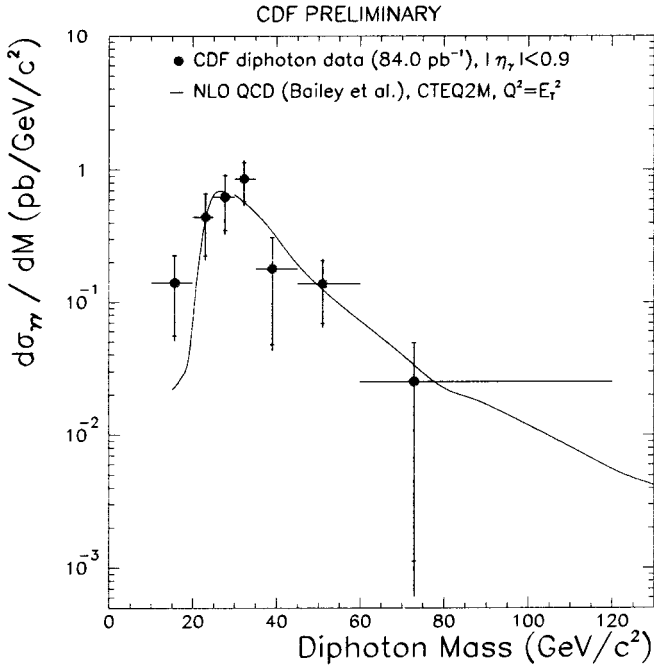
Fig. 4. The diphoton differential cross-section from CDF as a function of the diphoton invariant mass.

The diphoton mass spectra are in good agreement with the NLO QCD, and in the observed mass range there is no indication of a bump due to production of *e.g.* a new particle.

4. Inclusive jets

High transverse momentum jets are predominantly produced in proton–antiproton collisions by two body scattering of a single proton constituent with an antiproton constituent. Predictions for the inclusive jet cross-section [11] have been made using NLO QCD. These calculations to third order in the strong coupling constant α_s^3 reduce theoretical uncertainties, due to choice of renormalization scale (μ) to some $(10–20)\%$. Within the framework of conventional QCD, the study of the jet inclusive cross-section is also useful for extraction of the strong coupling constant. The cross-section for the production of jets is measured as a function of the jet energy transverse to the incident beams of the Tevatron Collider.

At low E_T jet production is dominated by gluon–gluon scattering, while at high E_T the main contribution comes from quark–quark scattering.

The inclusive jet cross-section at DØ [12] measured in rapidity range $|\eta| \leq 0.5$ and jet E_T range of (50–450) GeV is shown in Fig. 5. The data
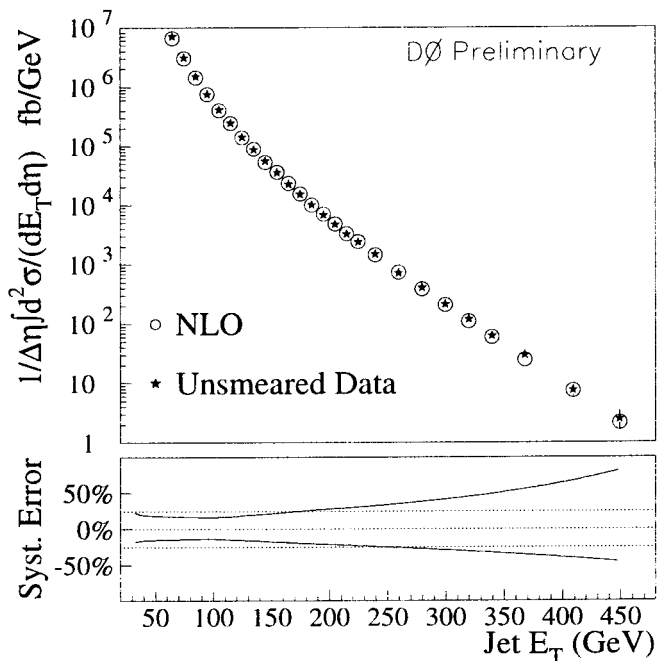

Fig. 5. A comparison of the central, $|\eta| \leq 0.5$, inclusive jet cross-section at DØ to a NLO QCD prediction. The points include statistical errors. The inset curves represent plus and minus 1 σ systematic error.

are for 91 pb^{-1}. The errors are statistical only and they are uncorrelated from point to point. There is an overall luminosity error of about 8%. The inset shows the total systematic error as a function of jet E_T. Figure 5 also shows a theoretical prediction from the NLO QCD [11]. A good agreement with theory is observed over the cross-section span of some seven orders of magnitude. The renormalization scale is $\mu = E_T/2$ where E_T is the maximum jet E_T in the generated event. The parton distribution function is CTEQ2ML [13]. Partons within R=1.2 radius of one another were clustered if they were also within R=0.7 of their weighted centroid in the $\eta - \phi$ space. Figure 6 shows the ratio of data(D)-theory(T) over theory, (D-T/T), for CTEQ2M, CTEQ2ML, and CTEQ3M [13] parton distribution functions. The CTEQ2M and CTEQ2M pdf's are derived from low-energy inelastic scattering data and from HERA ep data. The shape of the predictions with these pdf's is in excellent agreement with the data, as is the CTEQ2M normalization. In addition, the (1992–1993) data are in a good agreement
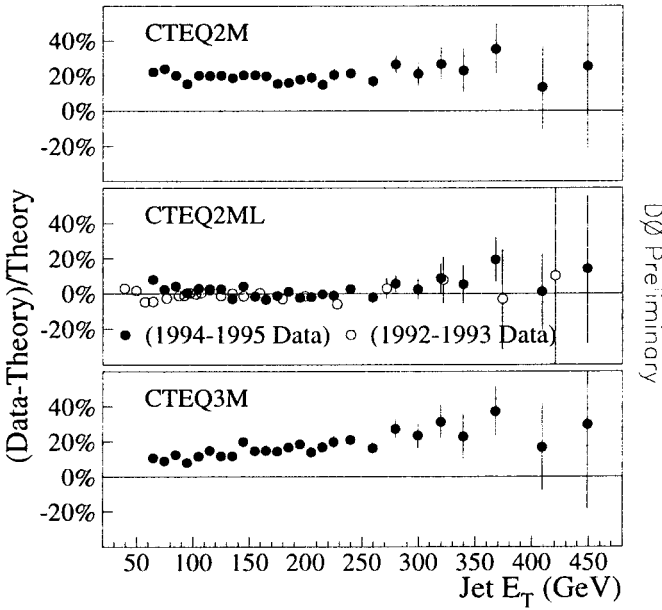
Fig. 6. Difference between DØ inclusive jet data and the NLO QCD prediction with three different parton distributions. The solid (open) symbols are for the (1994-95) and (1992-93) data, respectively.
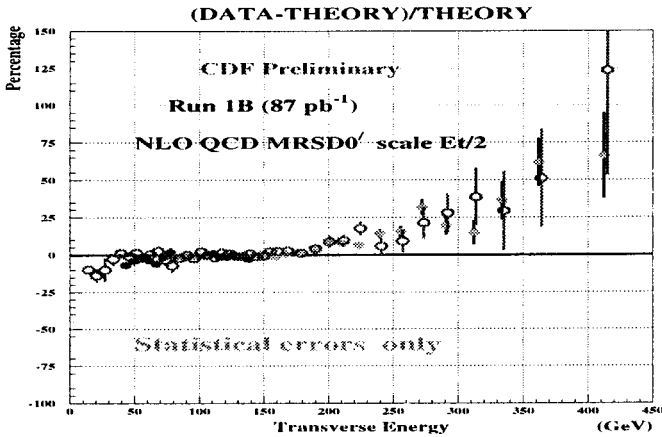

Fig. 7. Difference between CDF inclusive jet data and the NLO QCD prediction with MRSD parton distributions. The solid (open) symbols are for the (1994–95) and (1992–93) data, respectively.

with the (1994–1995) data as shown in central plot. For the CTEQ3M pdf's which include the deep inelastic data, recent HERA data, W boson asymmetry and Drell–Yan measurements, the theory underestimates the inclusive jet cross-sections from about 10% at low E_T to some 20% at the high E_T end.

CDF also collected two samples of inclusive jet data; one for 19.3 pb^{-1} from (1992–93) run and second one for 87 pb^{-1} from (1994–95) run. Data in both runs [14] (shown in Fig. 7) were taken in rapidity range of 0.1–0.7 and agree well with each other. After being corrected for energy smearing and scale [15], the data are compared to the NLO QCD with MRSD parton distributions with a $\mu = E_T/2$ renormalization scale. The error bars which are statistical only are shown for the 1992–93 run with lower luminosity. There is a good agreement between data and theory up to about 150 GeV of jet E_T. Above that energy, there is an increasing excess of data with respect to theory. For the highest jet E_T's the observed cross-section is about a factor of two higher than the predicted one. CDF estimates the maximum error on the cross-section due to corrections not to exceed some 20%, so it can hardly be used to explain the excess. Therefore, other possibilities such as choice of the pdf's are being investigated [16]. There may be other corrections to the NLO QCD theory (*e.g.* soft gluon resummation) to be considered as well. Another very intriguing possibility would be the assumption of a new resonant state production or perhaps a manifestation of the substructure of quark.

As the conclusions are based on the observation of a deviation of data from theory, it is interesting to compare the CDF and DØ data without their respective theories. This may help to determine if the potential source of a deviation is in the data itself or in the theory. A comparison of the CDF's run 1A data (19.3 pb^{-1}) with DØ run 1B data (91pb^{-1}) is shown in Fig. 8. The CDF data were first fit with a smooth curve and then data points for CDF (stars) and DØ (dots) are plotted after division by the fitted function. One can see that DØ data show small excess of cross-section in the range of 100–250 GeV and a deficit above 400 GeV. If DØ data however, were normalized to CDF's smooth curve in the range below 250 GeV the DØ defficiency range for high E_T jets would begin at much lower energies. The comparison of CDF and DØ data indicates that the high E_T jet excess at CDF, or lack of that excess at DØ , is likely to be due to some experimental problem and not necessarily due to theory.

An interesting idea to test QCD theory is based on a study of events with highest transverse energy. The topology of the hottest events and the sum jet E_T distribution may reveal [17] deviations from the QCD theory that may be less pronounced in other studies. This may be due to the fact that the sum E_T distribution is less dependent on the fragmentation processes.
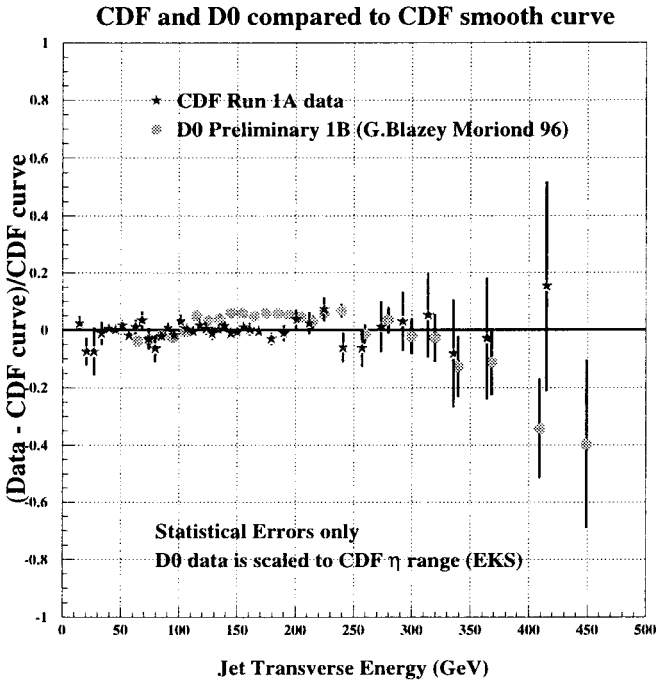
Fig. 8. Comparison of CDF and DØ inclusive jet data to the CDF smooth curve. The star symbols are for the CDF data and dot symbols are for DØ data.

While the DØ analysis is still in progress, CDF reported preliminary results of their study [14]. In Fig. 9 we show comparison of the event $\Sigma(E_T)$ cross-section ($\Sigma(E_T) \geq 400$ GeV) to the NLO (JETRAD + CTEQ3M) and the LO (HERWIG + CTEQ2L) theories. With both theories normalized to data at 400 GeV one observes growing deviation from data as $\Sigma(E_T)$ increases. This deviation appears to be little dependent on the choice of the physics generator and seems to be stronger than that observed with the inclusive jets.

The dijet angular and mass distributions have also been used as another test of the QCD theory, where deviations may be sensitive to new physics. Both, CDF [14] and DØ [12] have investigated dijet angular and mass distributions. Within available statistics, the dijet angular distribution shows no deviation with the quark compositeness scales up to 1.6 TeV. The dijet mass distribution from DØ [12] shows no deviation from the NLO QCD, while CDF's result [14] shown in Fig. 10 indicates a possibility of a small deviation at high mass end of this distribution. This is consistent with the CDF's inclusive jet and large $\Sigma(E_T)$ analyses but the strength of this devia-
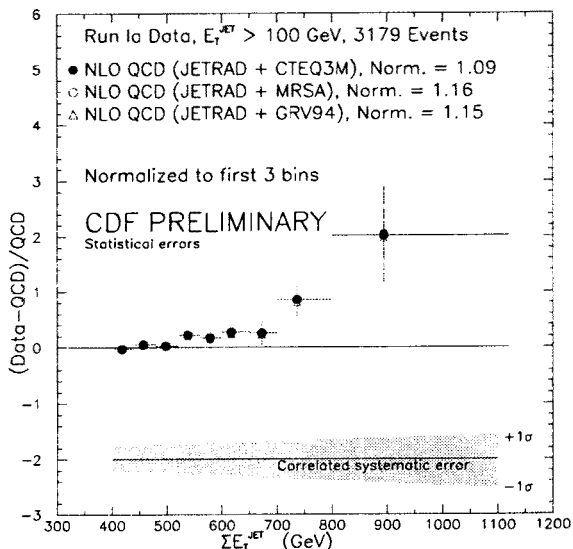
Fig. 9. The CDF's large $\Sigma(E_T)$ data compared to NLO QCD theory with three different parton distributions.
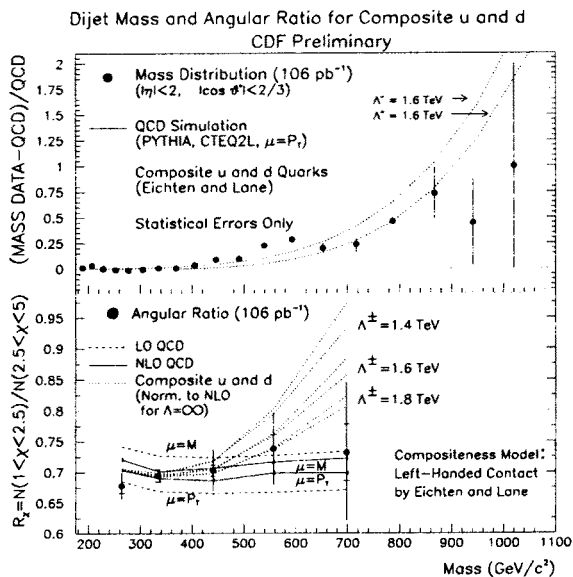

Fig. 10. The CDF's dijet mass and angular distributions compared to the QCD LO and NLO models with various quark compositeness scales.

tion is smaller than in the inclusive jet and large $\Sigma(E_T)$ data. Based on this observation it seems difficult to accomodate the inclusive jet, large $\Sigma(E_T)$, dijet mass and angular distributions with a common value for the compositeness scale. This may imply in turn, that if the excess in CDF's inclusive jets and large $\Sigma(E_T)$ data were indeed due to new physics, it would probably be not in agreement with the quark compositeness model of Ref. [18] where increase in high E_T dijet production was expected.

5. Test of scaling in QCD

An alternative test of QCD is to measure the inclusive jet cross-section at widely separated center of mass energies. The hypothesis of scaling suggests that the scaled jet cross-section, $E_T^4(E d^3\sigma/dp^3)$, is independent of $\sqrt{s}$ when plotted as a function of the variable $x_T = 2E_T/\sqrt{s}$. The QCD cross-sections depend, however, on the energy scale of the interaction (Q^2) suggesting that the cross-sections may not scale as expected. The running of the strong coupling constant and the evolution of the parton distribution functions are manifestation of the energy scale dependence of the interaction. In earlier measurement [19] at 546 GeV, CDF has excluded scaling for low E_T jets at 95% confidence level. Recently, both CDF [20] and DØ [21] measured the inclusive jet cross-section for $\bar{p}p$ interactions at the center of mass energy of 630 GeV. The data are well reproduced by the NLO QCD and MRSA pdf's above 40 GeV but confirm deviation from scaling for jets below some 40 GeV. It has been also found that the 630 GeV data differ from earlier UA2 result.

6. Ratio of $W+1$ jet to $W+0$ jets

Events with W boson and jets can be used to measure the ratio, R^{10}, of the production cross-sections for $W+1$ Jet to $W+0$ Jets events. This R^{10} ratio can be used in theoretical calculations to extract a value of the strong coupling constant at the mass of the W, $\alpha_s(M_W^2)$.

With 83 pb^{-1} in 1994-95 run, 36,891 $W \to e\nu$ candidates restricted to the central part of the calorimeter ($|\eta| \leq 1.1$) were detected at DØ [22]. With the jet E_T cut at 25 GeV there were 33,511 $W+0$ Jets and 2,841 $W+1$ Jet candidates. After subtracting the background contributions from multi-jet events and from other electroweak processes these numbers become 32,835 for $W+0$ Jets and 2,599 for $W+1$ Jet giving the value of R^{10} equal to about 0.08. A comparison of the R^{10} values with $E_T^{\min}$ ranging from 20 to 60 GeV to theoretical calculations using the DYRAD [23] Monte Carlo and the CTEQ3 family of pdf's is shown in Fig. 11. One can see that the theory is not only three standard deviations below the experimental result, but it

also exhibits little dependence on the value of α_s making the extraction of the strong coupling constant from this method impossible at present. It is speculated that origin of the problem may be due to a poor understanding of the gluon distribution in the proton.
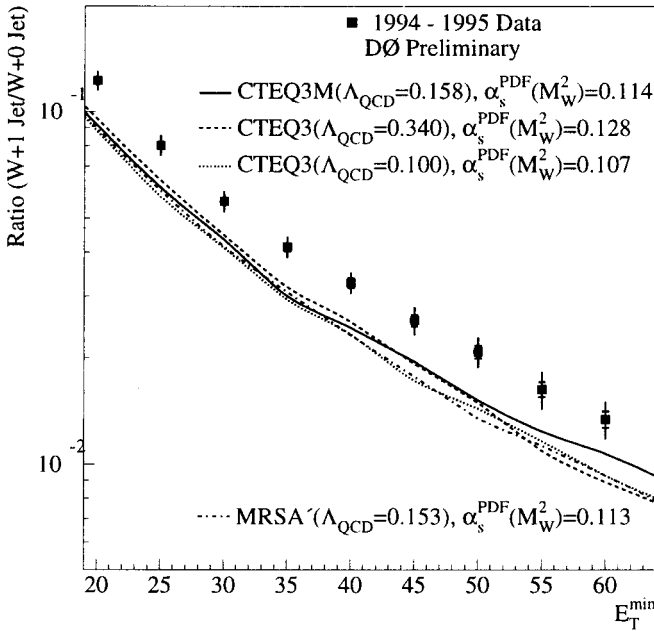

Fig. 11. The ratio R^{10} as a function of jet $E_{\rm T}$, $E_{\rm T}^{\min}$. The outer error bars are statistical and systematic added in quadrature. The solid curve is for the preferred CTEQ3M parton distributions, and the other CTEQ3 curves span the extrems in α_S. A calculation using the MRSA structure function is also plotted.

7. Diffractive production of jets and W's

The properties of elastic and diffractive scattering are well described by the phenomenology of pomeron exchange, where pomeron is a color singlet with quantum numbers of the vacuum [24]. It has been proposed that the observation of jets in diffractive events would probe the partonic nature of the exchanged pomeron. The pomeron is assumed to be either of hard structure derived from two gluons sharing the pomeron momentum, or soft structure like gluonic component of the proton. In collider experiments, the signature of a hard diffractive event is the presence of a rapidity gap, along with a hard scattering processes (jet production, W production, etc.). Since the pomeron is a color singlet, radiation is suppressed in events with

pomeron exchange, resulting typically in a large rapidity gap. The existence of a diffractive signal in the data may be observed as a larger number of rapidity gap events in the forward multiplicity distribution than expected from the non-diffractive background.

Both DØ [25] and CDF [26] observed the presence of forward rapidity gaps in events with high E_T jet production. The fraction of forward rapidity gap events observed is in excess of those expected to be produced from multiplicity fluctuations at both, 1800 GeV and 630 GeV center of mass energies. This result is consistent with expectations from the hard single diffractive jet production and provides the first experimental evidence for this process at $\sqrt{s} = 1800$ GeV. The forward gap fraction is found also to increase with the boost of the leading dijet system. There was also observed a class of events containing high E_T central jets and two forward rapidity gaps, consistent with a hard double pomeron exchange topology.

8. Other QCD studies

It is interesting to look for effects of interference between gluons, called often *color coherence*. Both CDF and D0 have explored gluon interference effects in three-jet events. The selected events have a rather hard leading jet ($E_T \geq 120$ GeV) and a soft third jet ($E_T \geq 10$ GeV). The distribution of the third jet direction around the second jet is used to investigate possible gluon interference. It turns out that physics simulators with gluon interference effects included (Herwig, Pythia) give a good description of the data. In addition, the NLO QCD theory, which has only leading order third-jet processes, is also in good agreement with data. This indicates that the observed interference effects are presumably perturbative in origin and present in the $2 \rightarrow 3$ matrix element of QCD.

To search for interference effects in the emission of much softer gluons (which will push the study into the non-perturbative regime), DØ has investigated [27] the energy flow around the jet and the W direction in W+Jet events. In this case the signal for interference results from a difference between the energy distribution on the W side (no color flow) and on the jet side, where the interference may occur between the outgoing parton and the incoming beam partons. Qualitatively, the data show the expected gluon interference, for example the energy flow is indeed relatively enhanced on the jet side between the outgoing jet and the beam direction but more study is needed to make firm quantative statements.

Another interesting study is the production of jets with large rapidity separation. The emission of soft gluons into the rapidity interval is described by the formalism of Balitsky, Fadin, Kuraev and Lipatov (BFKL) and it can be tested by measuring the decorrelation in azimuthal angle between the jets.

This decorrelation is a consequence of the gluon emission. The two jets most extreme in rapidity are selected and the mean value of $\cos(\pi - \Delta\phi)$ is plotted as a function of $\Delta\eta$. The data show increasing amount of decorrelation as $\Delta\eta$ increases. This effect appears to be not well described in the NLO QCD theory.

9. Summary and outlook

Large data sets are now available from both CDF and DØ detectors at the Tevatron. Although the analyses still continue, the overall QCD tests show good agreement with the QCD theory. A possible hint of disagreement between data and QCD in the high-E_T and large ΣE_T jet cross-sections is a challenge for experiments, but it also inspires theory to re-evaluate the parton distribution functions and other assumptions of the QCD model. In addition to above, application of other than cone-type jet algorithms (Nearest Neighbour, K_T, *etc.*), which allow jet size to vary, may be considered as more suitable approach in the analyses of jet data spanning over very wide energy range. This in turn, may bring new insights into QCD tests based on data from the Tevatron collider.

With the expected luminosity increase by two order of magnitudes for the Tevatron run II, much higher levels of precision will be achieved in collider data. This may include a possibility of an on-line calibration of jet energy response using large sample of jets from the *Top* quark and *W* boson to all jet decays, with mass of these objects known precisely from the study of their electro-weak decays. All of the above will lead in turn to more detailed tests of QCD, and perhaps observation of physics beyond the *Standard Model*.

REFERENCES

[1] F. Abe *et al.*, CDF Collab., *Nucl. Instrum. Methods* **A271**, 387 (1988).

[2] S. Abachi *et al.*, DØ Collab., *Nucl. Instrum. Methods* **A338**, 185 (1994).

[3] S. Abachi *et al.*, DØ Collab., subm. to 28th ICHEP, Warsaw, Poland, 1996.

[4] H. Baer, J. Ohnemus, J.F. Owens, *Phys. Rev.* **D42**, 61, (1994).

[5] F. Abe *et al.*, CDF Collab., subm. to 28th ICHEP, Warsaw, Poland, 1996.

[6] H. Baer, J. Ohnemus, J.F. Owens, *Phys. Lett.* **B234**, 127 (1990).

[7] H. Baer *et al.*, private communication, 1996.

[8] S. Abachi *et al.*, DØ Collab., subm. to DPF'96, Minneapolis 1996.

[9] B. Bailey, private communication, 1996.

[10] F. Abe *et al.*, subm. to 28th ICHEP, Warsaw, Poland, 1996.

[11] W.T. Giele, E.W.N. Glover, D.A. Kosower, *Phys. Rev. Lett.* **73**, 2019 (1994).

[12] S. Abachi *et al.*, DØ Collab., subm. to 28th ICHEP, Warsaw, Poland, 1996.

[13] H.L. Lai *et al.*, *Phys.Rev.* **D51**, 4763 (1995).

[14] F. Abe *et al.*, CDF Collab., subm. to 28th ICHEP, Warsaw, Poland, 1996.

[15] F. Abe *et al.*, *Phys. Rev. Lett.* **70**, 1376 (1992).

[16] H.L. Lai, W.K. Tung, MSU-HEP-60508, CTEQ-605, 1996.

[17] H. Piekarz, for D0 Collab.,*Proc. DPF'94* Albuquerque, 1192 (1994) and, H. Piekarz, J. Wightman, DØ Note 2315 (1995).

[18] E. Eichten, I. Hinchliffe, K. Lane, C. Quigg, *Rev. Mod. Phys.*, Vol. **56**, 579 (1984).

[19] A. Akopian, *et al.*, CDF Note 3656 (1996).

[20] F. Abe *et al.*, CDF Collab., subm. to DPF'96, Minneapolis, 1996.

[21] S. Abachi *et al.*, DØ Collab., subm. to DPF'96, Minneapolis, 1996.

[22] S. Abachi *et al.*, DØ Collab., subm. to 28th ICHEP, Warsaw, Poland.

[23] W.T. Giele, E.W.N. Glover, D.A. Kosower, *Nucl. Phys.* **B244**, 237 (1993).

[24] A. Donnachie, P.V. Landshoff, *Nucl. Phys.* **B267**, 690 (1986).

[25] F. Abe *et al.*, CDF Collab., subm. to 28th ICHEP, Warsaw, Poland, 1996.

[26] S. Abachi *et al.*, DØ Collab., subm. to 28th ICHEP, Warsaw, Poland, 1996.

[27] S. Abachi *et al.*, DØ Collab., subm. to 28th ICHEP, Warsaw, Poland, 1996.